Cell-Laden Nanocellulose/Chitosan-Based Bioinks for 3D Bioprinting and Enhanced Osteogenic Cell Differentiation

Panita Maturavongsadit, ^{1,5} Lokesh Karthik Narayanan, ^{2,3,5} Parth Chansoria, ^{2,5} Rohan Shirwaiker, ^{1,2,5} S. Rahima Benhabbour*^{1,4,5}

¹ Joint Department of Biomedical Engineering, North Carolina State University and The University of North Carolina at Chapel Hill, Chapel Hill, NC, USA

² Edward P. Fitts Department of Industrial and Systems Engineering, North Carolina State University, Raleigh, NC, USA

³ Department of Industrial and Manufacturing Engineering, North Dakota State University, Fargo, ND, USA

⁴ Division of Pharmacoengineering and Molecular Pharmaceutics, UNC Eshelman School of Pharmacy, University of North Carolina at Chapel Hill, Chapel Hill, NC, USA

⁵ Comparative Medicine Institute, North Carolina State University, Raleigh, NC, USA

*PI contact: benhabs@email.unc.edu, (919) 843-6142

Abstract

3D bioprinting has recently emerged as a very useful tool in tissue engineering and regenerative

medicine. However, developing suitable bioinks to fabricate specific tissue constructs remains a

challenging task. Herein, we report on a nanocellulose/chitosan-based bioink, that is compatible

with a 3D extrusion-based bioprinting technology, to design and engineer constructs for bone

tissue engineering and regeneration applications. Bioinks were prepared using thermogelling

chitosan, glycerophosphate, hydroxyethyl cellulose and cellulose nanocrystals (CNCs).

Formulations were optimized by varying the concentration glycerophosphate (80-300 mM),

hydroxyethyl cellulose (0-0.5 mg/mL), and CNCs (0-2% w/v) to promote fast gelation kinetics (<

7 s) at 37°C and retain the shape integrity of constructs post 3D bioprinting. We investigated the

effect of CNCs and pre-osteoblast cells (MC3T3-E1) on the rheological properties of bioinks,

bioink printability, and mechanical properties of bioprinted scaffolds. We demonstrate that the

addition of CNCs and cells (5 million cells/mL) significantly improved the viscosity of bioinks

and the mechanical properties of chitosan scaffolds post-fabrication. The bioinks were

biocompatible and printable at an optimized range of printing pressure (12-20 kPa) that did not

compromise cell viability. The presence of CNCs promoted greater osteogenesis of MC3T3-E1

cells in chitosan scaffolds as shown by the upregulation of alkaline phosphatase activity, higher

calcium mineralization and extracellular matrix formation. The versatility of this CNCs-

incorporated chitosan hydrogel makes it attractive as a bioink for 3D bioprinting to engineer

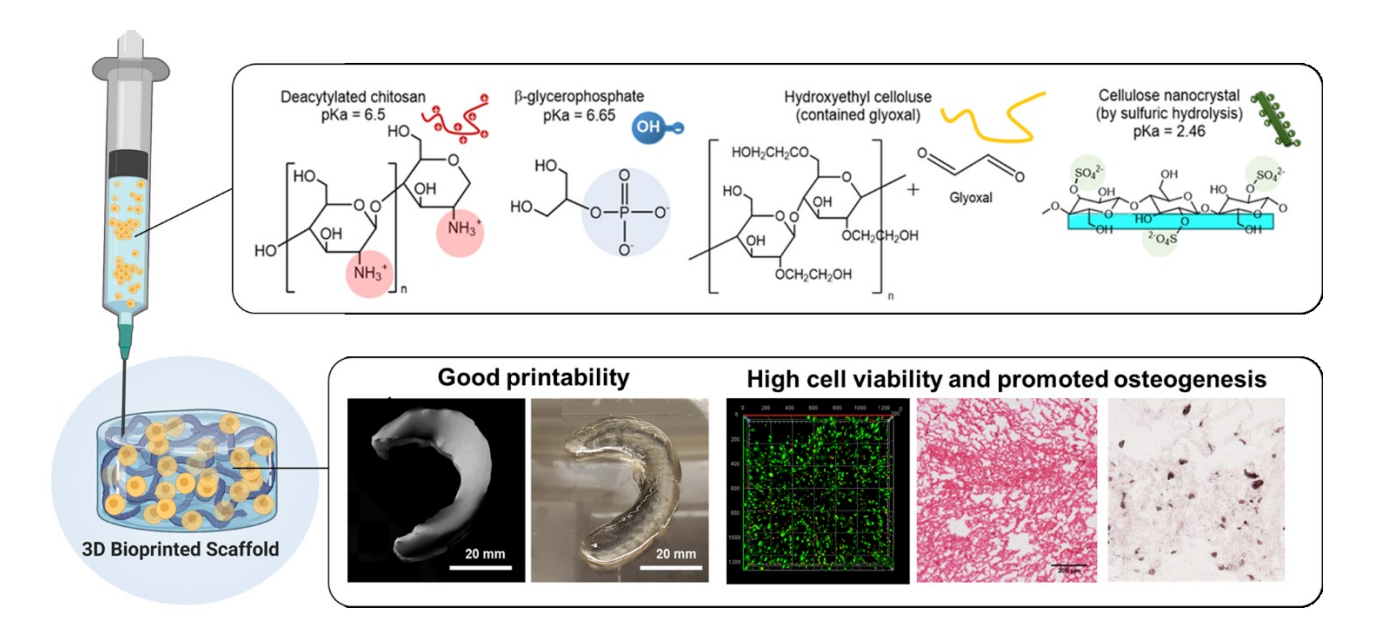
scaffolds for bone tissue engineering and other therapeutic applications.

Keywords: Chitosan-based hydrogel, cellulose nanocrystal, bioink, osteogenic differentiation,

bioprinting

2

Graphical abstract



1. Introduction

Three-dimensional (3D) bioprinting processes utilize additive manufacturing technologies to create a 3D scaffold or cellularized tissue construct made of laden cells and biomaterials referred to "bioinks". 3D bioprinting has shown significant promise in tissue engineering to restore or regenerate defected tissues due to its benefits over traditional acellular scaffold fabrication processes ¹⁻³. 3D bioprinting provides the ability to create biomimetic complex constructs in which different cell types can be precisely distributed at high densities within 3D scaffolds ^{4, 5}. The most common bioprinting techniques for processing bioinks are inkjet ⁶⁻⁸, acoustic ^{9, 10}, laser-induced forward transfer ^{11, 12}, and extrusion-based methods ¹³⁻¹⁵. Among these approaches, extrusion-based bioprinting has proven to be the most versatile technology owing to its compatibility with bioinks of a broad range of viscosities that can be used to engineer clinically translational tissue-engineered scaffolds ^{16, 17}. However, there continues to be a need to design bioinks tailored to achieve optimal printability and functionality for a given application, particularly for bone tissue engineering applications ¹⁸⁻²¹.

When designing bioinks, natural polymers are generally preferred over synthetic polymers owing to their biocompatibility, biodegradability, cell affinity and ability to mimic properties of the natural extracellular matrix (ECM). Natural polymer-based hydrogels, including alginate ²²⁻²⁴, gelatin ²⁵⁻²⁷, fibrin ²⁸, hyaluronic acid ^{29, 30}, and collagen ³¹, are the most common polymers investigated as bioink matrices for extrusion-based bioprinting, and can support osteogenic differentiation. However, these materials have low mechanical properties that cannot mimic the bone microenvironment to effectively promote bone formation ^{32, 33}. Herein, we aimed to develop a new bioink formulation for 3D bioprinting with superior mechanical properties that mimic the bone microenvironment and better support bone formation.

We recently developed a tunable thermo-/pH-responsive chitosan hydrogel incorporated with cellulose nanocrystals (CNCs) as an injectable biomaterial for encapsulation of pre-osteoblasts (MC3T3-E1 cells) for minor bone fractures repair ³⁴. Chitosan has been widely used in bone tissue engineering applications ³⁵⁻⁴¹. In our previous injectable system, the formulation was prepared using chitosan, CNCs, β-glycerophosphate and hydroxyethyl cellulose (HEC) ³⁴. This system is thermo-sensitive and can form hydrogels instantly within 7 s at 37°C through a mechanism that involves hydrophobic interactions within the chitosan network and hydrogen bonding between chitosan and CNCs. We demonstrated that the CNCs-incorporated chitosan-based formulations were biocompatible, supported cell encapsulation and viability, and were injectable through a 20G needle without compromising cell viability ³⁴. Importantly, CNCs had a significant impact on the mechanical properties of the hydrogel and on differentiation and behavior of pre-osteoblasts encapsulated within the hydrogel. CNCs significantly improved the mechanical properties of the chitosan gel to closely mimic the bone microenvironment, and promoted cell spreading within the hydrogel compared to chitosan-only hydrogels ³⁴. The goal of this work was to develop, for the first time, CNCs-incorporated chitosan-based formulations as bioinks for 3D extrusion-based bioprinting of cell-laden scaffolds to promote osteogenic differentiation and bone regeneration. As such, these bioink formulations are designed to fabricate patient-specific bone tissue-engineered scaffolds for critical-size bone defects regeneration.

Bioink formulations were optimized by investigating a range of CNCs and HEC concentrations. Formulations, placebo or cell-encapsulated, were characterized and optimized for their rheological properties (viscosity, yield stress, and storage modulus recovery) to determine the ability to use these bioinks in 3D printing and the ability to fabricate scaffolds that can retain their shape and size fidelity. Printability of optimized bioink formulations and fidelity of the final

3D bioprinted constructs were assessed using a custom computer-aided design (CAD) tool path. Storage modulus and Young's modulus of bioprinted constructs were determined to assess the impact of CNCs and cells on the mechanical properties of bioprinted scaffolds. Additionally, cell viability post-printing was determined using a Live/Dead cell staining and DNA quantification assay. The impact of bioink formulations on cell differentiation was also evaluated using an alkaline phosphatase activity assay and corroborated with collagen and calcium histological staining. These results provide a strong toolbox for the development of bioinks and determining the required optimal bioprinting parameters to engineer robust and customized 3D complex bone tissue-engineered constructs that can mimic native tissues and effectively promote repair of large bone defects.

2. Experimental Section

2.1. Materials

All bioink compositions including chitosan (CS, 85% deacetylated, 200-800 cP, 1 wt% in 1% acetic acid), β-glycerophosphate (BGP), and cotton cellulose (Whatman® ashless filter-aid paper) were obtained from Sigma-Aldrich. Dulbecco's modified eagle media (DMEM) was purchased from Corning. Sulfuric acid, dialysis membrane (SnakeSkin® dialysis tubing with MWCO 7,000 Da), hydroxyethyl cellulose (HEC), and phosphate buffer saline (PBS) were purchased from Sigma-Aldrich. Fetal bovine serum (FBS) was purchased from Atlanta Pharmaceuticals. Paraformaldehyde and Tween20 were purchased from ThermoFisher Scientific. Luer-Lock connectors were purchased from Baxter.

2.2. In vitro cell culture

MC3T3-E1 cells (ATCC CRL-2593, Manassas, VA, USA), a pre-osteoblast cell line isolated from mouse calvaria, is a model cell line used for the formulation of bioinks and the study of cell viability and osteogenesis of cells encapsulated in 3D bioprinted scaffolds. Cells were cultured in complete growth media containing DMEM with 10% FBS under 5% CO₂ at 37°C. MC3T3-E1 cells were trypsinized by 0.25% trypsin solution with EDTA (Gibco, Carlsbad, CA, USA), followed by centrifugation at 3000 rpm, 25°C for 5 min to obtain a cell pellet. Subsequently, the cell pellet was resuspended in serum-free DMEM media and mixed with other bioink excipients to formulate bioinks (the detailed formulation is described below).

2.3. Preparation of bioink formulations

A 3% (w/v) CS solution was prepared by stirring CS powder in 1% (v/v) aqueous acetic acid at room temperature overnight. BGP, glycerol, and CNCs were used in their powder forms. CNCs were synthesized using our previously reported procedure 34 . MC3T3-E1 cells were prepared following the method mentioned in section 2.2. *In-situ* CS-CNCs bioinks were formulated by first mixing the formulation excipients in three separate vials under aseptic conditions at a final volume of 1 mL. The first vial contained a 3% w/v CS solution in 0.1 M aqueous acetic acid (667 μ L). The second vial contained 1M BGP gelling agent solution (100 μ L), and the third vial contained a solution of MC3T3-E1 cells (5 million cells), HEC, and CNCs in DMEM media (213 μ L). The first two solutions were mixed together using a luer-lock connector to create a neutral CS solution (pH \sim 6.8), followed by centrifugation at 4000 rpm, 25°C for 5 min to remove any air bubbles present in the formulation. Subsequently, the neutral CS solution was combined with the rest of

the components in vial three and homogenously mixed to obtain the final bioink formulation for 3D bioprinting.

2.4. Rheological properties of bioinks

DHR-3 Rheometer (TA Instruments, New Castle, DE, USA) was used to characterize the viscosity, yield stress, storage modulus recovery, and gelling kinetics. All tests were conducted at 25°C with a gap of 500 µm. The 3% w/v CS solution was used to optimize all testing protocols (n=3). Viscosity curves were determined by a logarithmic shear rate sweep from a shear rate of 0.1 s⁻¹-100 s⁻¹ with 10 points per decade. The yield stress was determined by an oscillatory shear strain sweep from 0.1% to 2000% at a frequency of 1 Hz with 5 points per decade, and the yield stress was defined as the shear stress at the crossover point of the storage (G') and loss (G") moduli. The storage modulus recovery was determined by three phases of oscillatory shearing at a frequency of 1 Hz after a 5-min soak time where no stress was applied. In phase 1, materials were exposed to a constant shear strain at 1% for 2 minutes to determine an initial storage modulus. In phase 2, 30 s of high shear strain at 2000% (above the material's yield stress to mimic extrusion and flow through a bioprinter nozzle) was applied; and finally, in phase 3, materials were exposed to another constant shear strain at 1% for 2 minutes. The initial storage modulus was calculated from the average storage moduli measured in the initial 2 min of the material being exposed to 1% shear strain (phase 1). The recovered storage modulus was determined as the storage modulus 10 s after the shear strain transitioned from 2000% back to 1% (phase 3). The percent recovery was defined as

 $\frac{\text{Recovered storage modulus}}{\text{Initial storage modulus}} \times 100$

The bioink gelling kinetics were determined using dynamic time sweep. Briefly, a bioink formulation (50 μ L) was poured into the parallel plate instrument and the measurement was conducted at 37°C, an angular frequency (ω) of 10 rad/s, and a strain amplitude of 0.01%. The gelation time was determined for each sample (n=3) as a time of crossover of storage modulus (G') and loss modulus (G") for each sample.

2.5. Scanning electron microscopy (SEM) imaging

The microstructure of acellular and cell-laden casted scaffolds was analyzed using scanning electron microscopy (SEM) imaging. To investigate the effect of CNCs and cells on scaffolds' microstructure, samples were prepared as previously described above in section 2.3 and incubated at 37°C in 2 mL of DMEM media for 24 h. At the end of the experiment, scaffold samples were removed from the media, flash frozen with liquid nitrogen, and lyophilized for 24 h (SP VirTis Advantage XL -70, Warminster, PA, USA). The lyophilized samples were subsequently cross-sectioned, sputter-coated with gold-palladium alloy (60:40) (Hummer X Sputter Coater, Anatech USA, Union City, CA, USA), and imaged using a Zeiss Supra 25 field emission scanning electron microscope (Carl Zeiss Microscopy, LLC, Thornwood, NY, USA) following our previously reported procedure ³⁴.

2.6. 3D printing of bioinks

Key printing parameters (pressure, speed, and layer height) were optimized for all extrudable bioink formulations selected from screening studies detailed in Supplementary Sections 1 and 2 (S1 and S2). Three (3) mL of the optimized bioink was loaded into the print-head of an extrusion

bioprinter (BioX, Cellink, Gothenburg, Sweden) with a 20-G nozzle and printed following a custom tool path with multiple directional changes (**Figure S1**). Images of the printed strands were captured after a 3-min gelling time using a digital camera (EOS 80D, Canon, Tokyo, Japan) and assessed for feature resolution.

2.7. Mechanical properties of 3D bioprinted scaffolds

Bioinks without and with MC3T3-E1 cells (5 million/mL) were prepared using the method detailed in section 2.3. Subsequently, solid cylindrical scaffolds (8 mm diameter × 2 mm thickness) were printed with optimized parameters onto a petridish using a BioAssemblyBot[®] (Advanced Solutions, Louisville, KY, USA) fitted with a 20-G nozzle (**Figure 1**). Prior to mechanical analysis, the bioprinted scaffolds were incubated in DMEM media in a 24-well tissue culture plate at 37°C for 24 h.

To determine storage modulus, dynamic rheology measurements were performed using a DHR rheometer fitted with a parallel plate geometry. The strain amplitude was set as 1% for all measurements, which was within the linear viscoelastic region of the hydrogel formulation. Dynamic frequency sweep testing (0.1–20 rad/s) was performed at 37°C to determine the storage modulus of the fabricated 3D printed scaffolds (n=3). To determine Young's modulus, compression tests were performed using a RSAIII micro-strain analyzer (TA Instruments, New Castle, DE, USA) fitted with a parallel plate geometry. The analyses were performed with a 35 N load cell and a strain rate of 0.01 mm/s for 45 s.

2.8. Shrinkage properties of 3D bioprinted scaffolds

The degree of swelling of bioprinted scaffolds with and without MC3T3-E1 cells (5 million/mL) was determined by measuring the weight of a sample before (W_{initial}) and after incubation in DMEM media at 37°C for 24 h (W_{24h}). Solid cylindrical bioprinted scaffolds (7.5 mm diameter × 4 mm thickness, n=4) were printed with optimized printing parameters into a 24-well tissue culture plate using a BioAssemblyBot[®] fitted with a 20-G nozzle. The degree of shrinkage was calculated using the following equation:

Degree of shrinkage (%) =
$$[(W_{initial} - W_{24h})/W_{initial}] \times 100$$

Additionally, the diameter (d) and thickness (h) of scaffolds after 24h incubation were measured using a caliper, and the estimated volume was calculated using the following formula:

$$V = \pi \times (d/2)^2 \times h$$

2.9. In vitro cell viability and proliferation in the 3D bioprinted scaffolds

Bioink formulations seeded with MC3T3-E1 cells (5 million/mL) were prepared under aseptic condition as described in section 2.3. Subsequently, solid cylindrical scaffolds (5 mm diameter \times 3 mm thickness, n=5) were printed directly into a 24-well tissue culture plate using a BioAssemblyBot® fitted with a 20-G nozzle. The same printing parameters were applied to all bioink formulations (pressure = 20 kPa, speed = 0.2 mm/s). For comparison and to determine the effect of 3D bioprinting on cell viability, 3D cell-laden scaffolds were casted into a 24-well tissue culture plate and used as controls. Cell viability in 3D bioprinted and direct casted scaffolds was determined using Live/Dead cell staining kit (Molecular Probes, Eugene, OR, USA). After 24 h incubation at 37°C, the cell-laden scaffolds were stained with Live/Dead assay reagent containing 1 μ M Calcein AM and 2 μ M ethidium homodimer (EthD) for 45 min at 37°C. Scaffolds were

subsequently washed thrice with pre-warmed PBS. The labeled cells were viewed simultaneously under a laser scanning confocal microscope (Zeiss LSM700, White Plains, NY, USA) by collecting five Z-stacks with a 5x lens for each sample.

Cell proliferation within 3D bioprinted scaffolds was determined using the Quanti-iT PicoGreen dsDNA Assay (Molecular Probes, Eugene, OR, USA). At days 3 and 7, samples were rinsed with PBS and exposed to 1% Triton X-100 (Sigma-Aldrich, Saint Louis, MO, USA) followed by three freeze-thaw cycles in order to lyse the cells. Cell lysates were diluted with TE buffer (200 mM Tris-HCL, 20 mM EDTA, pH 7.5) and mixed with PicoGreen reagent according to the manufacturer's protocol. A BioTek Cytation 5 fluorospectrometer plate reader was utilized to quantify the fluorescence of each sample (ex. 480 nm, em. 520 nm).

2.10. In vitro osteogenic differentiation

Bioinks seeded with MC3T3-E1 cells (5 million/mL) were used to fabricate solid cylindrical scaffolds using the aforementioned 3D bioprinting procedure. Scaffolds (n=5) were subsequently cultured in osteogenic media (containing 10% FBS, 1x P/S, 50 μg/mL ascorbic acid-2 phosphate, 10 nM dexamethasone). At predetermined endpoints (days 7, 14 and 21), the samples were analyzed for alkaline phosphatase (ALP) activity, calcium mineralization, and ECM formation.

2.10.1. Alkaline phosphatase (ALP) activity

Cell-encapsulated bioprinted scaffolds (n=5) were rinsed with PBS and exposed to 1% Triton X-100 followed by three freeze-thaw cycles in order to lyse the cells. Cell lysates were used to quantify the ALP activity by an Alkaline Phosphatase Assay Kit (BioVision, Milpitas, CA, USA). In brief, $20~\mu L$ of cell lysate was combined with $50~\mu L$ of p-nitrophenyl phosphate (pNPP) solution in the assay buffer. The mixture was incubated for 1 h at room temperature, protected from light. The reaction was quenched by adding $20~\mu L$ of stop solution, and the absorbance of the resulting solution was measured at 405~nm using a plate reader. 1% Triton X-100 incubated with pNPP and the stop solution was used as a blank reference to calculate the absorbance for each sample. The absorbance value was converted to the concentration of p-nitrophenyl (pNP) using a standard curve of pNP (0–20 nmol/mL) generated by pNPP that was dephosphorylated by the ALP enzyme. ALP activity was reported as pNP content normalized by DNA count.

2.10.2. Histological staining

Calcium mineralization and extracellular matrix formation were analyzed by Von Kossa and hematoxylin and eosin (H&E) histological staining kit (Abcam, Cambridge, MA, USA). Samples were fixed in 4% paraformaldehyde (pH 7.3), dehydrated in sucrose solutions, and embedded in OCT fixing reagent. Samples were then cryo-sectioned at 10 µm thickness. Sample sections were stained with Von Kossa and H&E based on established manufacturer protocols and analyzed by light microscopy (Olympus BX61, Melville, NY, USA) with 5x and 10x lenses. Percent area of calcium mineralization and ECM formation in 3D bioprinted scaffolds were quantified using ImageJ software.

2.11. Statistical analysis

All data were represented as mean \pm standard deviation (SD) and analyzed with GraphPad Prism (version 8.4.2) using the one-way and two-way analysis of variance (ANOVA). The confidence levels were set as 90% (p* < 0.1), 95% (p** < 0.05) and 99% (p*** < 0.01).

3. Results and Discussion

3.1. CS-CNCs bioink formulations for 3D bioprinting

Composition and crosslinking process of bioinks are critical parameters that dictate biocompatibility, printability, and mechanical properties of 3D bioprinted scaffolds. In this study, we report on a CS-based hydrogel formulation containing CNCs ³⁴ and its optimization as a bioink for scaffold fabrication using 3D bioprinting. The physical/chemical properties of bioink formulations were optimized to improve their compatibility with the 3D bioprinting process used and offer a microenvironment that can support cell survival and accelerate osteogenic differentiation. The optimized bioink formulations illustrated in Table 1 were composed of MC3T3-E1 cells, CS, BGP, CNCs and HEC. The mechanism of CS-CNC gel formation involves a combination of hydrophobic interactions between the CS molecules, and chemical crosslinking via Schiff-base linkages between CS and HEC ³⁴. A seeding cell (MC3T3-E1) density of 5 million cells/mL was selected for its relevance to bone tissue formation in vitro and in vivo 42-44. BGP was used at a concentration of 100 mM to achieve optimum osmolality (~350 mOsmol/kg) for cell encapsulation and to promote gel formation at body temperature (37°C) 45, 46 (Figure 1). HEC, containing glyoxal groups, was incorporated in the bioink formulation at an optimized concentration of 0.1 mg/mL to enhance shape fidelity retention of 3D bioprinted scaffolds. The glyoxal groups in HEC act as a chemical crosslinker to covalently crosslink the CS backbone via

a Schiff-base reaction between the CS amine groups and HEC aldehyde groups ^{41, 47}. Unlike other CS-based bioinks reported in the literature ^{26, 48-50}, in this study, CNCs were incorporated at concentrations ranging from 0.5-1.5% w/v and used as a reinforcing agent to enhance the mechanical properties of 3D bioprinted scaffolds through hydrogen bonding between CS and CNCs. CNCs concentrations ranging from 0.5%-1.5% w/v were selected based on the printability of the resulting bioink formulations, combined with enhanced mechanical properties of the resulting bioprinted scaffolds compared to CS only bioinks. The 1.5% w/v CNCs was the highest concentration that allowed continuous printing without inducing any clogging during the extrusion process. On the other hand, using concentrations of CNCs below 0.5% w/v did not result in bioprinted scaffolds with significantly improved mechanical properties compared to CS only formulations. Details of formulation screening process and optimization are described in Supplementary Sections 1 and 2 (S1 and S2). The CS-CNCs bioink was transferred into a bioink cartridge for 3D printing, then gelled by temperature stimulation at 37°C on the printing plate (Figure 1).

Table 1. Optimized formulations of CS-CNCs bioinks used for the studies.

Hydrogel	CS (% w/v)	Gelling agent		_ CNCs	MC3T3-E1
		BGP (mM)	HEC (mg/mL)	(% w/v)	density (million cells/mL)
CS	2	100	0.1	0	0
CS+0.5%CNCs	2	100	0.1	0.5	0
CS+1.5%CNCs	2	100	0.1	1.5	0
CS-Cells	2	100	0.1	0	5
CS+0.5%CNCs-Cells	2	100	0.1	0.5	5
CS+1.5%CNCs-Cells	2	100	0.1	1.5	5

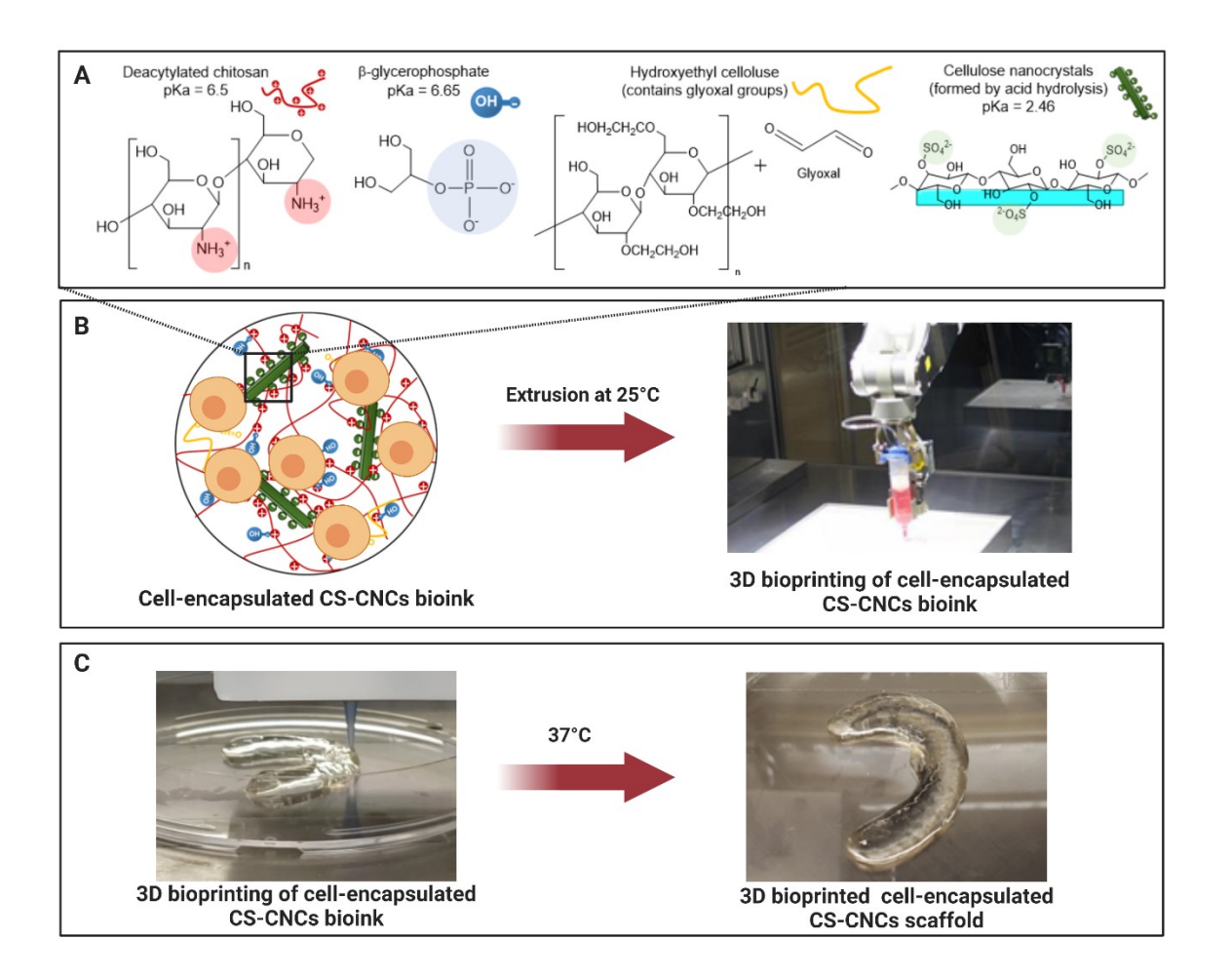


Figure 1. Schematic illustration of the 3D bioprinting process. **A)** Bioink formulation consisting of CS, BGP, HEC, and CNCs seeded with cells. **B)** Cell-encapsulated bioink was loaded into 3D-bioprinter cartridges and bioprinted onto a cell-culture glass coverslip with cartridge temperature controlled at 25°C. **C)** 3D bioprinted scaffold of a patient derived knee meniscus using CS-CNCs placebo bioink. The bioprinted scaffold was spontaneously gelled on a glass printing plate by temperature stimulation at 37°C. Part of the figure reproduced from Materialia, 100681, Maturavongsadit, P.; Paravyan, G.; Shrivastava, R.; Benhabbour, S. R., Thermo-/pH-Responsive Chitosan-Cellulose Nanocrystal Based Hydrogel with Tunable Mechanical Properties for Tissue Regeneration Applications, Copyright 2020 with permission from Elsevier.

3.2. Rheological properties of CS-CNCs bioinks

Rheological measurements were carried out to characterize the viscosity, yield stress, storage modulus recovery, and gelling kinetics of the developed bioinks. These properties are important parameters that determine the ability to use a bioink in 3D printing and the ability to fabricate scaffolds that can retain their shape and size fidelity, relative to the initial CAD dimensions, post 3D printing. The ideal rheological properties targeted for bioink formulations include 1) viscosity in the range of $30 - 6 \times 10^4$ Pa.s to support shape fidelity after printing ⁵¹⁻⁵³, 2) shear-thinning properties to allow flow under high shear stress ⁵¹⁻⁵³, 3) adequate storage modulus recovery to regain the original viscoelastic properties after deformation, and 4) fast gelling kinetics to retain the original CAD dimensions in the final 3D bioprinted structure ⁵¹⁻⁵³.

The viscosity of bioink formulations were measured to investigate the influence of CNCs and cells presence on rheological properties of bioink formulations. The viscosity of each bioink formulation was determined by flow sweep analysis. Results showed that all bioink formulations exhibited a shear thinning behavior with increasing shear rates compatible with extrusion-based 3D bioprinting ^{45,54} (**Figure 2A**). For acellular bioinks, presence of CNCs resulted in a slightly increased initial viscosity (106.09 ± 6.23, 117.78 ± 13.61 and 136.29 ± 10.52 Pa.s for CS, CS+0.5%CNCs, and CS+1.5%CNCs bioinks respectively). For cell-laden bioinks (5 million cells/mL), there was a significant increase in viscosity for all formulations (251.88 ± 3.81, 241.49 ± 28.96, and 258.90 ± 10.93 Pa.s in CS-cells, CS+0.5%CNCs-cells, and CS+1.5%CNCs-cells bioinks respectively) compared to their placebo bioink analogues (p < 0.1). At a frequency of 1 Hz, complex viscosity of acellular CS, CS+0.5%CNCs and CS+1.5%CNCs bioinks was approximately 14, 18, and 16 Pa.s respectively. For cell-encapsulated bioinks, the complex viscosity increased to 23, 32, and 42 Pa.s for CS, CS+0.5%CNCs and CS+1.5%CNCs bioinks

respectively (**Figure 2B**, **Table 2**). These results demonstrated that the presence of cells and CNCs in the bioink formulations resulted in a significant increase in initial viscosity likely due to increased volume fraction ^{54, 55} and presence of electrostatic interactions between the CS backbones in the bioink formulation. However, the effect imparted by cells was greater than the effect imparted by the CNCs owing to higher volume fraction in the presence of cells ⁵⁴.

Yield stress of bioink formulations, defined as an applied stress at which the bioink starts to flow as liquid, was characterized to predict the shape fidelity of scaffolds after printing. Results showed a slight increase in yield stress in the presence of CNCs; however, this increase was not significantly different (p > 0.1) (**Figure 2C, Table 2**). Likewise, incorporating cells did not change the yield stress of the bioinks compared to their cell-free analogues. The bioinks exhibited a yield stress in the range of 400 to 585 Pa.

The storage modulus recovery of bioink formulations was also determined as an indicator of the ability to retain the original CAD dimensions in the final 3D printed scaffolds. After 10 s of applied high shear strain above the material's yield stress, all acellular bioinks (CS, CS+0.5%CNCs, and CS+1.5%CNCs) exhibited similar high percent storage modulus recovery of over 75% (p > 0.1) (**Figure 2D, Table 2**). For cell-encapsulated bioinks (5 million cells/mL), the percent storage modulus recovery was decreased by ~20% in CS bioink (from 95.54% \pm 16.61% to 71.72% \pm 6.55%), and by ~15% in both CS-CNCs bioinks (from 76.00% \pm 3.53% to 62.36% \pm 11.15% Pa in CS+0.5%CNCs; and from 85.27% \pm 3.26 to 69.62% \pm 14.54% Pa in CS+1.5%CNCs); however, these differences were not statistically significant (p > 0.1). This effect by cells could be attributed to the relatively large size of MC3T3-E1 cells (~30-40 μ m) relative to the bioink network. As a result, this can lead to hindrance or delay in the self-healing process of

CS polymer and CS-CNCs network, limiting the ability of bioinks to recover their original properties.

The gelling kinetics of bioinks were determined by investigating the bioink transition between storage modulus (G') and loss modulus (G"). When gelled at 37°C, the G' for all bioink formulations instantaneously increased above the transition stage (a time of crossover of G' and G") within 7 s of the first detected time point, indicating fast gelation time for all formulations (less than 7 s) (Figure 2E, Table 2). This demonstrated that the presence of cells and CNCs did not significantly impact the gelation time of bioinks. However, it is worth noting that the impact of cells on the properties of bioinks and scaffolds will vary depending on cell density, polymer types and additives in the formulation ^{56, 57}. For example, Skardal *et al.* found that cell density above 25 million cells/mL led to failure in gelation of hyaluronan-based hydrogels ⁵⁶. Similarly, Buckley *et al.* showed that the addition of chondrocyte cells at 10 and 40 million cells/mL decreased the dynamic modulus of agarose hydrogels ⁵⁷.

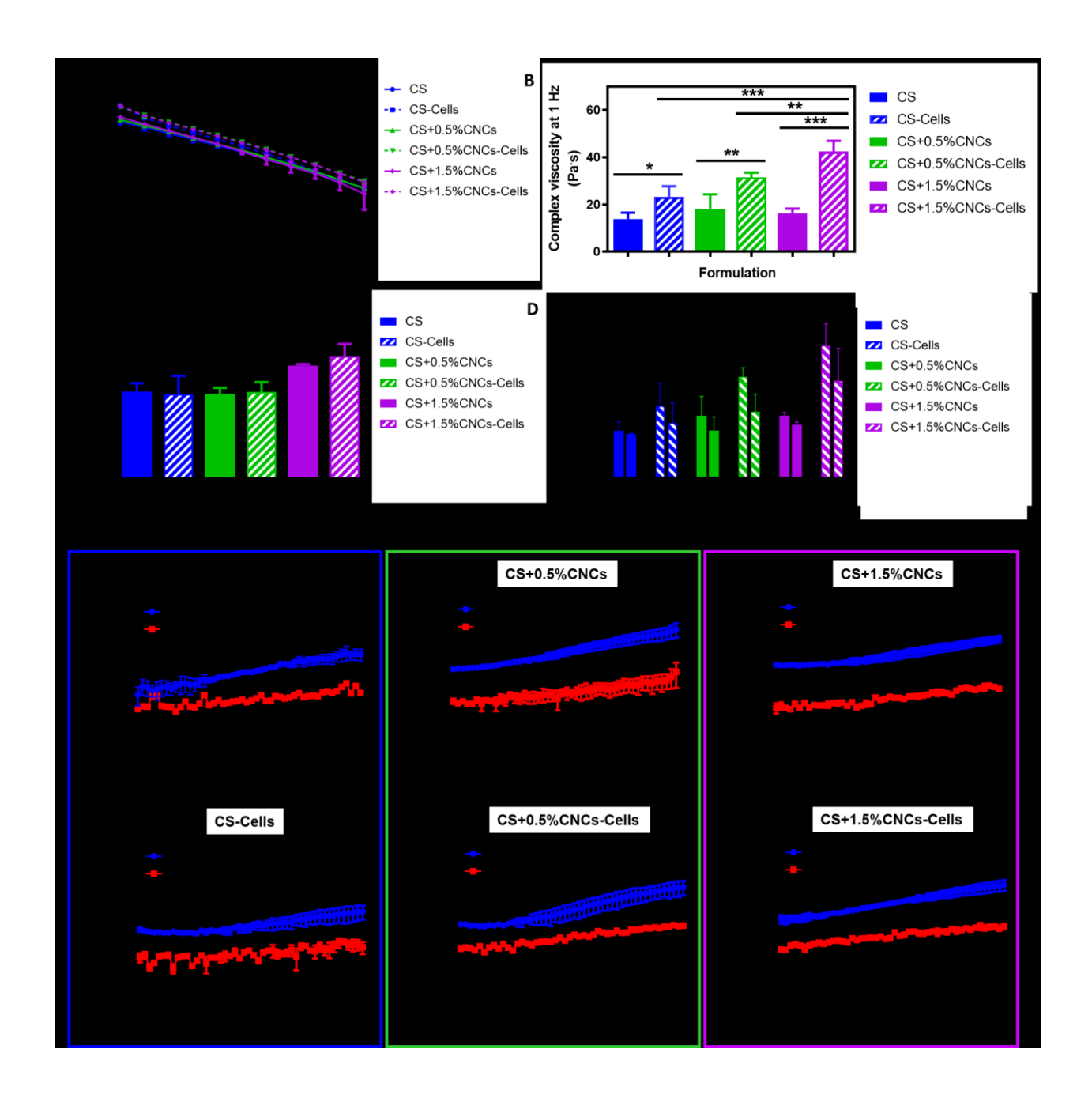


Figure 2. Rheological properties of CS-based bioinks containing different CNCs concentrations, without or with cells encapsulated at 5 million cells/mL (n=3). **A)** Viscosity curve of bioinks determined at a shear rate ranging from 0-100 s⁻¹. **B)** Complex viscosity of bioinks determined at a frequency of 1 Hz. Statistical analysis: ANOVA with Tukey's multiple comparisons tests, *p < 0.1, **p < 0.05, ***p < 0.01. **C)** Yield stress of bioinks determined by an oscillatory shear strain sweep from 0.1% to 2000% at a frequency of 1 Hz. Statistical analysis: ANOVA with Tukey's

multiple comparisons tests, *p < 0.1. **D)** Storage modulus recovery of bioinks illustrating the recovered storage modulus after undergoing 2000% strain for 30 s compared to their initial modulus. **E)** Gelling kinetics of bioinks using dynamic time sweep conducted at 37° C, an angular frequency (ω) of 10 rad/s, and a strain amplitude of 0.01% (n=3).

Table 2. Summary of rheological properties of bioinks. The values represent the mean (n=3) with their standard deviations.

Rheological properties	CS	CS-Cells	CS+0.5%CNCs	CS+0.5%CNCs- Cells	CS+1.5%CNCs	CS+1.5%CNCs- Cells
Viscosity (Pa.s) at 1 HZ	13.95 ± 2.66	23.16 ± 4.57	18.17 ± 6.11	31.56 ± 1.97	16.06 ± 2.10	42.45 ± 4.54
Yield stress (Pa)	$412.35 \pm \\ 45.35$	$403.16 \pm \\90.20$	401.93 ± 34.46	413.18 ± 50.59	536.68 ± 12.86	585.21 ± 61.77
Modulus recovery (%)	95.54 ± 16.61	71.72 ± 6.55	76.00 ± 3.53	62.36 ± 11.15	85.27 ± 3.26	69.62 ± 14.54
Gelation time (s)	< 7	< 7	< 7	< 7	< 7	< 7

3.3. 3D bioprinting of CS-CNCs bioinks

For each bioink formulation, optimal extrusion pressure, speed and needle height offset that resulted in continuous strands with consistent width following a custom tool path were determined (**Figure 3A**). A digital camera was used to capture the fidelity of printed strands after a 3-min gelling interval at 37°C. All bioink formulations exhibited consistent printed strands without breaking or detaching when fabricated under optimized printing conditions (**Figure 3A, B**). Bioinks containing CNCs (CS+0.5%CNCs and CS+1.5%CNCs) required greater extrusion pressure (20 kPa) to enable uniform printing of strands compared to CS-only bioinks (12 kPa).

While presence of cells in CNCs-containing bioinks did not require greater extrusion pressure compared to their acellular analogues (20 kPa), greater pressure (15 kPa) was required for cell-encapsulated CS bioinks compared to their acellular counterparts (12 kPa) (**Figure 3B**). Notably, it was found that using concentrations of CNCs greater than 1.5% w/v resulted in clogging of the extrusion nozzle and inability to utilize these formulations in a continuous extrusion-bioprinting process.

This printability data demonstrated that cell-encapsulated CS-CNCs bioinks exhibited good printability properties. The data also demonstrate that the minimum requirement for rheological properties of bioinks for 3D extrusion bioprinting can be different for each specific polymer-based bioink system. Our results showed that the CS-based bioinks had viscosities ranging between 100 and 250 Pa.s and exhibited shear-thinning properties compatible with extrusion-based 3D bioprinting ^{45, 54}. In addition, the bioinks exhibited a yield stress in the range of 400 to 585 Pa and percent storage modulus recovery above 60%, which was sufficient to support the printability and fidelity of scaffolds post 3D bioprinting. In contrast, for hyaluronic- and pluronic-based bioinks, the storage modulus recovery of bioinks are required to be above 85% in order to offer a good 3D bioprinting fidelity ⁵⁸⁻⁶⁰.

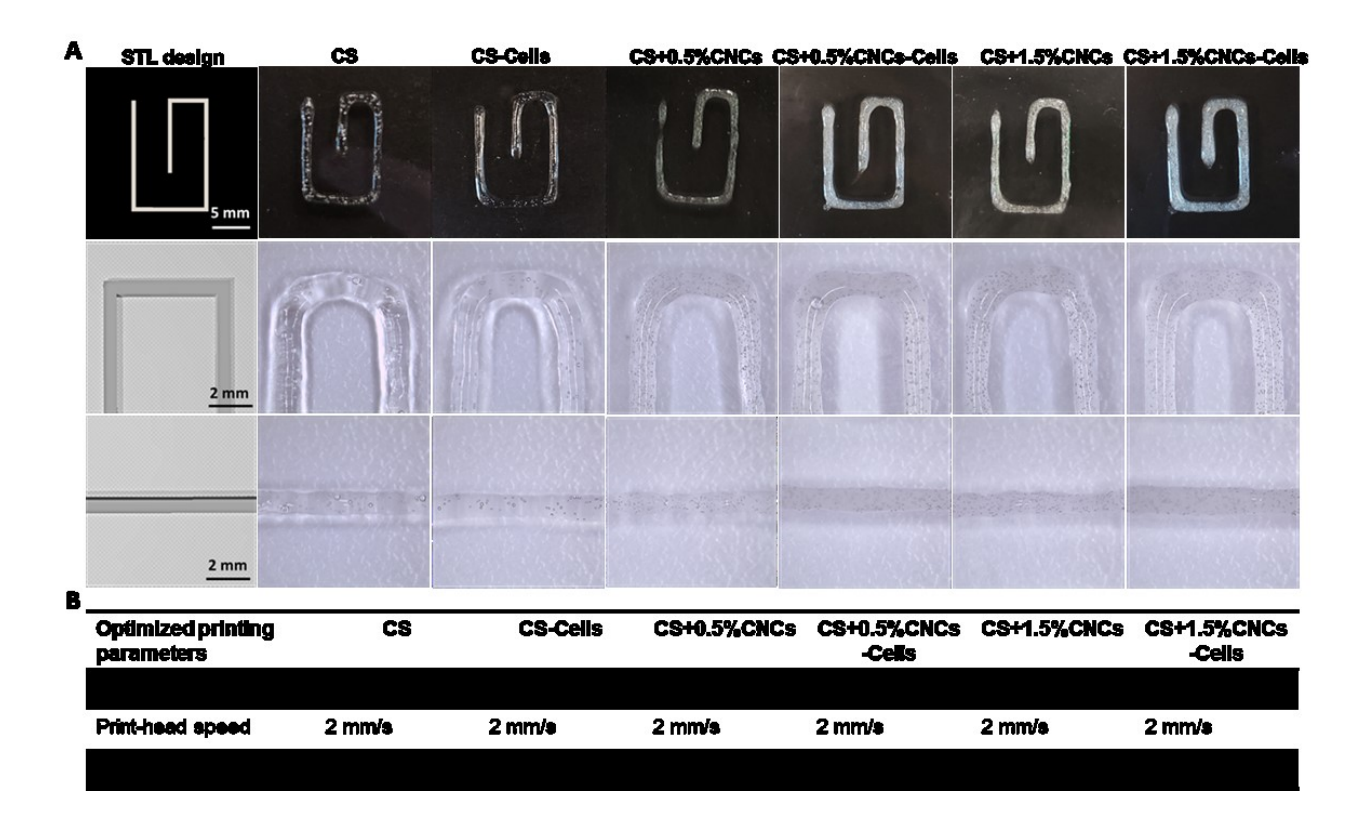


Figure 3. Printability of CS-based bioinks containing different concentrations of CNCs, without or with cells encapsulated at 5 million cells/mL (n=3). **A)** Images of strands 3D printed using different bioink formulations compared to the original CAD file. **B)** Optimized printing parameters for the fabrication of 3D bioprinted strands represented in (**A**).

3.4. Mechanical properties

One of the key characteristics of a well-designed bioink is its ability to generate high fidelity bioprinted scaffolds with good mechanical properties to support bone regeneration. Mechanical properties were investigated by determining the Young's modulus (E') and storage modulus (G') of scaffolds post 3D bioprinting from the stress-strain curves (**Figure 4**). Results showed that the presence of cells did not have a significant impact on the Young's modulus for all bioprinted

scaffolds (CS, CS+0.5%CNCs, and CS+1.5%CNCs, p > 0.1). However, the storage modulus of scaffolds containing CNCs was significantly higher in the presence of cells and was ~1.4 and 1.7 folds greater for CS+0.5%CNCs and CS+1.5%CNCs, respectively, compared to their acellular counterparts (p < 0.01) (**Figure 4B, C**). Additionally, the data showed that the presence of CNCs had a significant impact on both the Young's modulus and storage modulus. For formulations containing CNCs at 0.5 and 1.5% w/v, the Young's modulus was ~1.4 and 1.5 folds higher respectively compared to CS-only scaffolds (p < 0.01) (**Figure 4C**). Similarly, the storage modulus of bioprinted scaffolds was ~1.2 folds higher for CS-CNCs scaffolds compared to CS-only scaffolds (p < 0.01). These results demonstrated that the presence of CNCs significantly improved the mechanical properties of bioprinted scaffolds owing to interactions between CNCs and CS at 37° C 34 .

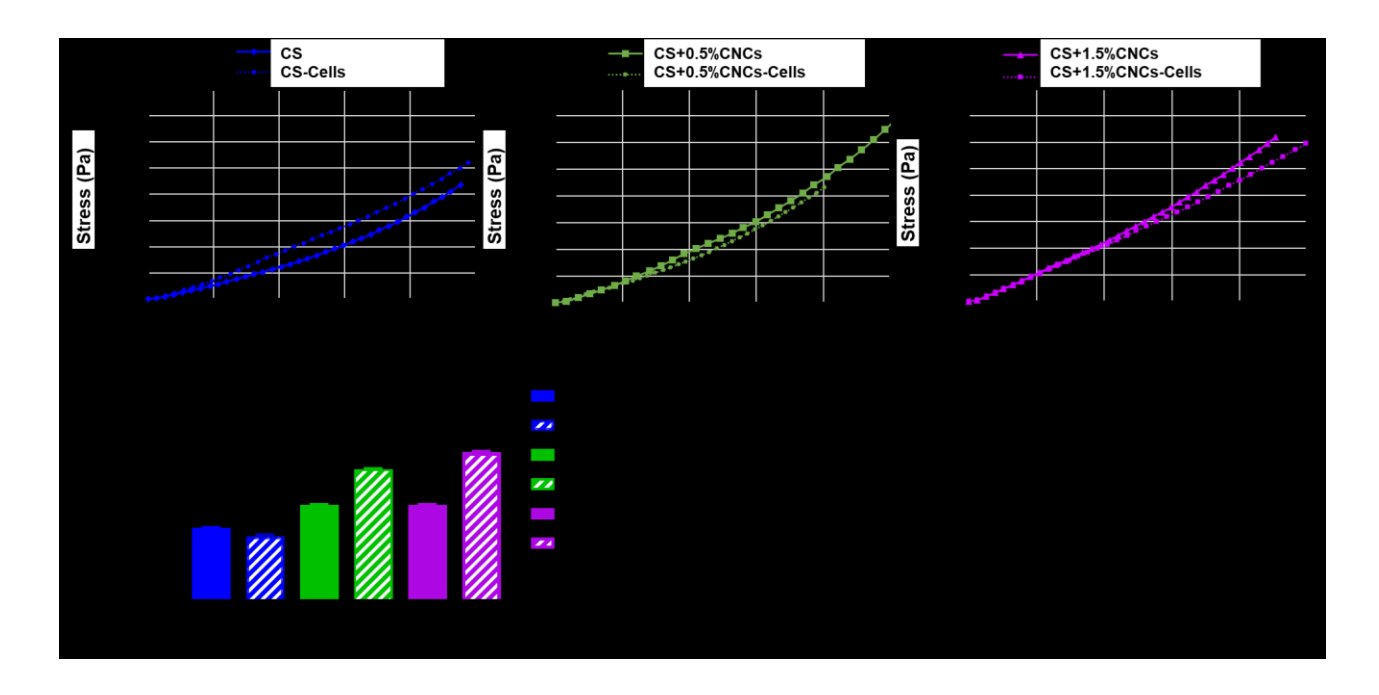


Figure 4. Mechanical properties of 3D bioprinted scaffolds after a 24 h incubation in tissue culture DMEM media at 37°C. **A)** Young's modulus (E') of 3D bioprinted scaffolds without and with MC3T3-E1 cells (5 million cells/mL) determined using compression test with a 35 N load cell and

a strain rate of 0.01 mm/s for 45 s. **B)** Storage modulus (G') of 3D bioprinted scaffolds without and with MC3T3-E1 cells (5 million cells/mL) determined using an a 2% amplitude strain and frequency range of 0.1-20 rad/s. **C)** Summary of the mechanical properties of different 3D bioprinted scaffolds represented in (**A-B**). The values represent the means (n=3) and standard deviations. Statistical analysis: ANOVA with Tukey's multiple comparisons tests, ***p < 0.01.

3.5. Shrinkage and microstructure analyses

Physical properties of bioprinted scaffolds, including degree of shrinkage and microstructure, are important to determine shape fidelity of bioprinted scaffolds and degree of diffusivity of scaffolds to support cell survival. The impact of cells and CNCs presence on the degree of shrinkage and microstructure of scaffolds were investigated after a 24h incubation in DMEM at 37°C. The shrinkage of bioprinted scaffolds in PBS (pH 7.4) at 37°C is attributed to an entropy-driven process of the disruption of both ionic interactions between CS and BGP and hydrophobic interactions within the CS network ³⁴. Results showed that the presence of cells in bioink formulations did not have a significant impact on the degree of shrinkage of the fabricated scaffolds. The degree of shrinkage ranged between 30-34% in all scaffolds (Figure 5A). The microstructures of scaffolds fabricated with or without cells showed high porosity with similar characteristics in all bioink formulations with no evident differences noted (Figure 5B). These results imply that the aforementioned entropy-driven process that governs the degree of shrinkage was not influenced by the presence of CNCs and cells during the first 24 h of incubation. All bioprinted scaffolds exhibited similar degree of shrinkage with high porosity to support the diffusivity of nutrients and molecules.

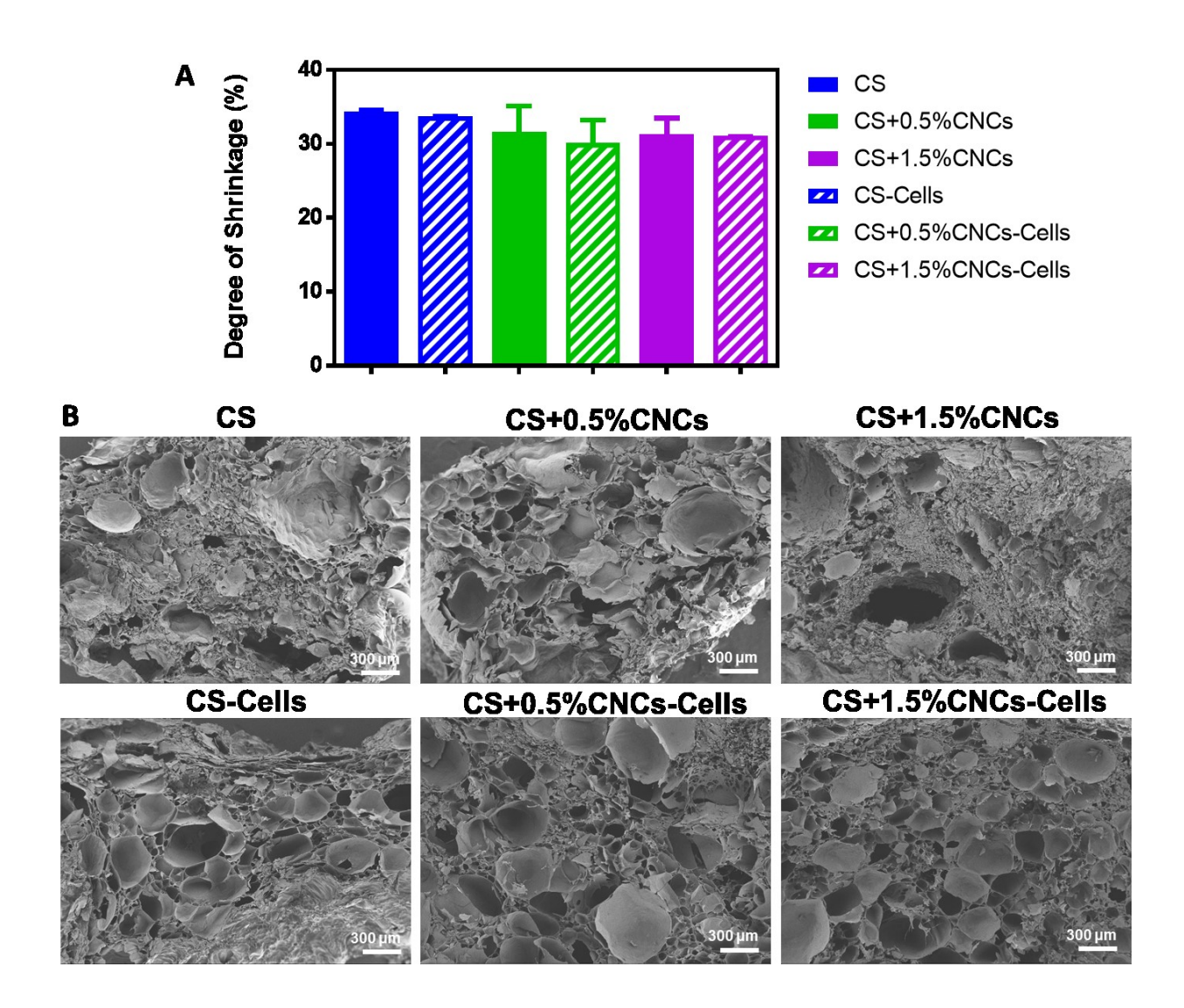


Figure 5. Physical properties of 3D cylindrical bioprinted scaffolds. **A)** Degree of shrinkage of cylindrical bioprinted scaffolds (n=4) fabricated using different bioink formulations without and with MC3T3-E1 cells (5 million cells/mL) determined after a 24 h incubation in DMEM at 37°C. Statistical analysis: ANOVA with Tukey's multiple comparisons tests, no statistical difference (p > 0.1). **B)** Microstructure of casted scaffolds imaged after a 24 h incubation in DMEM at 37°C.

3.6. In vitro cell-based assays

3.6.1. Cell viability and proliferation

Cell viability was used to assess the efficiency of the 3D bioprinting process and biocompatibility of bioink formulations. Previously, we reported that CS-CNCs formulations were biocompatible and supported the persistence of MC3T3-E1 cells over 7 days in complete growth media ³⁴. Herein, cell viability was qualitatively evaluated by imaging living cells and dead cells encapsulated within bioprinted scaffolds after 24 h incubation in complete media at 37°C. Cell viability was also assessed in casted scaffolds as a control. Results comparing cell viability in casted scaffolds and 3D bioprinted scaffolds showed similar cell viability in both scaffolds, demonstrating that the printing process did not impact cell viability (**Figure 6A**). These results demonstrate that the extrusion pressure used during the 3D bioprinting process (12-20 kPa) was compatible with cell survival ⁶¹⁻⁶³. Cell proliferation was further quantified using a Quant-iT PicoGreen dsDNA assay after 3 and 7 days incubation in complete media at 37°C. Results showed that for all scaffolds there was no significant cell proliferation after 7 days incubation at 37°C and the presence of CNCs did not alter cell viability and proliferation in the bioprinted scaffolds (p > 0.1) due to lack of adhesion motifs ⁶⁴⁻⁶⁶ (**Figure 6B**).

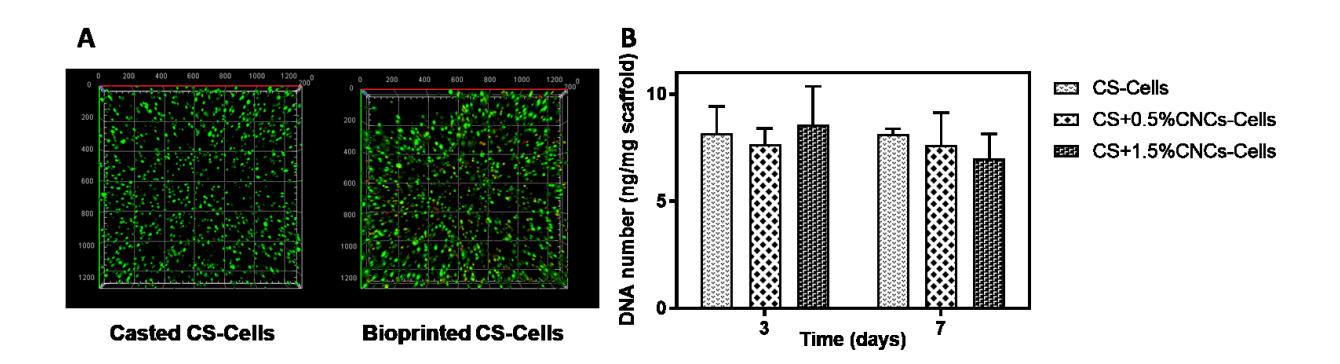


Figure 6. In vitro cell viability and proliferation assay assessing cell-encapsulated 3D bioprinted scaffolds. **A)** Cell viability in 3D bioprinted CS scaffolds compared to casted scaffolds after 24 h

incubation in complete media at 37°C using Live/Dead cell staining assay and Z-stack imaging with a 5x lens. Living cells are depicted in green and dead cells are depicted in red. **B)** Proliferation of cells encapsulated in bioprinted scaffolds fabricated using different bioink formulations (n=5). DNA number was quantified using Quant-iT PicoGreen dsDNA assay at day 3 and 7 incubation in complete media at 37°C. Statistical analysis: ANOVA with Tukey's multiple comparisons tests, no statistical difference (p > 0.1).

3.6.2. Osteogenic differentiation

To investigate the potential use of CS-CNCs bioink for bone tissue engineering applications, cell-laden bioprinted scaffolds were cultured in osteogenic media for 21 days. Osteogenesis was first investigated by determining alkaline phosphatase (ALP) enzyme activity as an indicator in the early stage of osteogenic differentiation. Results showed a peak value in ALP activity at day 7 and for all scaffolds tested (CS, CS+0.5%CNCs, CS+1.5%CNCs) with a significantly higher activity observed for the CS+1.5%CNCs bioprinted scaffolds. In comparison, in CS and CS+0.5%CNCs scaffolds, ALP activity reached a peak value at day 14 and this activity was retained up to day 21. These results demonstrate that with the highest concentration of CNCs (CS+1.5%CNCs) bioprinted scaffolds exhibited a faster onset of osteogenesis compared to CS only and CS+0.5%CNCs scaffolds.

ECM formation was assessed using H&E staining. The extent of ECM formation (stained in red) in all types of cell-laden scaffolds increased over time with the highest percent area of ECM obtained with the CS+1.5%CNCs scaffolds at day 14 and 21 (**Figure 7B**, **D**). While the extent of ECM in CS+0.5%CNCs scaffolds at day 14 was significantly higher than in CS scaffolds, there

was no significant difference in ECM extent in these two scaffolds at day 21 (**Figure 7D**). Calcium mineralization was further examined by Von Kossa staining to assess the impact of CNCs in bioprinted scaffolds on osteogenesis performance. The results illustrated in **Figure 7C**, **E** and **Figure S4**, show no calcium content or calcium mineralization after 7 days incubation in osteogenic culture. Calcium deposition in cells increased at day 14 in all scaffold formulations. At day 21, the extent of calcium deposition was significantly increased and covered larger areas in all scaffolds. As demonstrated in **Fig 7E** the area of mineral deposits within the scaffold was significantly higher in CS+1.5%CNCs scaffold at days 14 and 21 compared to CS and CS+0.5%CNCs scaffolds (**Figure 7E**). The collective increase in osteogenic markers observed with CS+1.5%CNCs scaffolds could be attributed to the significantly higher mechanical properties imparted by CNCs ⁶⁷.

Collectively, this data supports the development of CS-CNCs based bioinks to engineer 3D bioprinted constructs for bone tissue engineering. The versatility of these formulations provides the ability to fine-tune the rheological and mechanical properties for 3D bioprinting and the mechanical and structural integrity of bioprinted scaffolds. Future studies will investigate in vivo efficacy of the CS-CNCs scaffolds in fracture heading. In addition, we will investigate incorporating osteoconductive and osteoinductive molecules to further improve these bioink formulations for bone tissue engineering and regeneration applications.

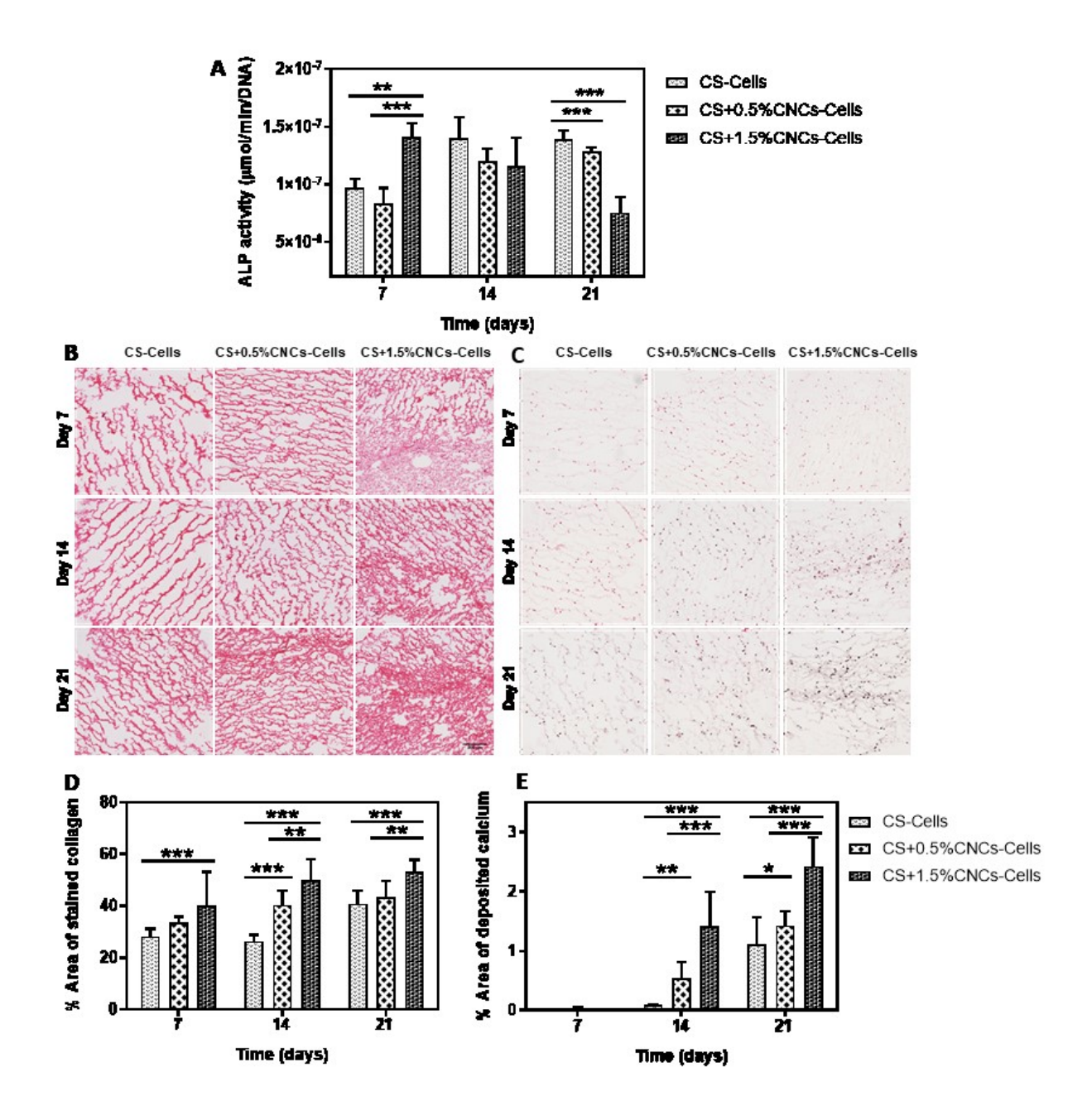


Figure 7. In vitro osteogenesis assays in 3D bioprinted scaffolds (n=5). **A)** ALP activity measured using the p-nitrophenyl phosphate (pNPP) assay at day 7, 14 and 21 post-incubation in osteogenic culture conditions. **B)** H&E staining of newly formed ECM in bioprinted scaffolds evaluated at day 7, 14 and 21 post-incubation in osteogenic culture conditions. All images share the same scale bar of 200 μm. **C)** Von Kossa staining of calcium mineralization in bioprinted scaffolds collected at day 7, 14 and 21 post-incubation in osteogenic culture conditions. All images share the same

scale bar of 200 μ m. **D)** Percent area of newly formed ECM in bioprinted scaffolds quantified by ImageJ at day 7, 14 and 21 post incubation in osteogenic culture conditions. **E)** Percent area of calcium mineralization in bioprinted scaffolds quantified by ImageJ at day 7, 14 and 21 post-incubation in osteogenic culture conditions. Statistical analysis: ANOVA with Tukey's multiple comparisons tests, *p < 0.1, **p < 0.05, ***p < 0.01.

4. Conclusion

In summary, we report for the first time the development of a CS formulation containing CNCs as a bioink for 3D extrusion-based bioprinting. The CS-CNCs bioinks lent themselves well to extrusion-based 3D bioprinting and effectively promoted osteogenic differentiation. The composition and crosslinking process of bioink formulations were optimized to allow efficient printability. The impacts of CNCs and pre-osteoblast cells on viscosity, yield stress and storage modulus recovery of bioink formulations were investigated, to provide the ability to predict 3D bioprinting outcomes. The mechanical properties of 3D bioprinted CS scaffolds were significantly improved by incorporating CNCs and cells. All bioink formulations were biocompatible and supported cell encapsulation at a high density of 5 million cells/mL. More importantly, CS-CNCs scaffolds significantly promoted osteogenic differentiation as demonstrated by accelerated early activity of alkaline phosphatase, calcium mineralization and collagen formation in ECM. We envision that this bioink will support the development of biomimetic bioprinted constructs with target properties that can match native bone tissues to effectively repair bone defects.

Supporting information

Detail of optimization of CS-CNCs bioink formulations (S1); Details of formulation parameters

investigated for optimization (Table S1); Optimization of 3D bioprinting parameters (S2);

Computer-aided design (CAD) model used to investigate printability of CS-CNCs bioink

formulations (Figure S1); 3D bioprinted CS scaffolds using different CAD geometries (Figure S2);

Mechanical properties of bioprinted scaffolds measured after 2h incubation at 37°C (without any

media or PBS) (Figure S3); Von Kossa staining of calcium mineralization within bioprinted

scaffolds (20x magnification) analyzed at day 14 and 21 post-incubation in osteogenic culture

conditions (Figure S4).

Corresponding Author

*Contact: benhabs@email.unc.edu, (919) 843-6142

Author Contributions

Conceived and designed the experiments: SRB, PM, RS and LKN.

Performed the experiments: PM, LKN, PC.

Contributed reagents/materials/analysis tools: SRB, RS

Wrote the paper: SRB and PM.

Declaration of Competing Interest

SRB and PM are inventors on a patent application related to this work filed by the University of

North Carolina, Office of Technology Commercialization (UNC OTC) (PCT International

32

Application PCT/US2019/034492, filed on May 30, 2019 and U.S. Provisional Patent Application No. 62/679,334, filed on June 1, 2018). The authors declare no conflict of interest.

Acknowledgments

This work was supported by the NC Translational and Clinical Sciences (NC TraCS) Institute, which is supported by the National Center for Advancing Translational Sciences (NCATS), National Institutes of Health (grant award number 2KR1031802 to PM). This work was also supported by the Eshelman Institute for Innovation (EII), UNC Eshelman School of Pharmacy (grant RX03912404 to SRB and RAS) and the US National Science Foundation (CMMI 1652489 to RAS).

Data availability. All other data supporting the findings of this manuscript are available from the corresponding author (S.R.B) upon reasonable request.

References

- 1. Mironov, V.; Boland, T.; Trusk, T.; Forgacs, G.; Markwald, R. R., Organ printing: computer-aided jet-based 3D tissue engineering. *Trends Biotechnol.* **2003**, *21* (4), 157-161.
- 2. Chan, B. P.; Leong, K. W., Scaffolding in tissue engineering: general approaches and tissue-specific considerations. *Eur. Spine J.* **2008**, *17 Suppl 4*, 467-79.
- 3. Langer, R.; Tirrell, D. A., Designing materials for biology and medicine. *Nature* **2004**, 428 (6982), 487-492.
- 4. Rutz, A. L.; Hyland, K. E.; Jakus, A. E.; Burghardt, W. R.; Shah, R. N., A Multimaterial Bioink Method for 3D Printing Tunable, Cell-Compatible Hydrogels. *Adv. Mater.* **2015,** *27* (9), 1607-1614.
- 5. Derby, B., Printing and Prototyping of Tissues and Scaffolds. *Science* **2012**, *338* (6109), 921-926.

- 6. Campbell, P. G.; Weiss, L. E., Tissue engineering with the aid of inkjet printers. *Expert opinion on biological therapy* **2007**, *7* (8), 1123-1127.
- 7. Saunders, R. E.; Derby, B., Inkjet printing biomaterials for tissue engineering: bioprinting. *Int. Mater. Rev.* **2014**, *59* (8), 430-448.
- 8. Hutchings, I. M.; Martin, G. D., *Inkjet technology for digital fabrication*. John Wiley & Sons: 2012.
- 9. Demirci, U.; Montesano, G., Single cell epitaxy by acoustic picolitre droplets. *Lab on a Chip* **2007**, 7 (9), 1139-1145.
- 10. Fang, Y.; Frampton, J. P.; Raghavan, S.; Sabahi-Kaviani, R.; Luker, G.; Deng, C. X.; Takayama, S., Rapid generation of multiplexed cell cocultures using acoustic droplet ejection followed by aqueous two-phase exclusion patterning. *Tissue Engineering Part C: Methods* **2012**, *18* (9), 647-657.
- 11. Guillotin, B.; Souquet, A.; Catros, S.; Duocastella, M.; Pippenger, B.; Bellance, S.; Bareille, R.; Rémy, M.; Bordenave, L.; Amédée, J., Laser assisted bioprinting of engineered tissue with high cell density and microscale organization. *Biomaterials* **2010**, *31* (28), 7250-7256.
- 12. Guillotin, B.; Guillemot, F., Cell patterning technologies for organotypic tissue fabrication. *Trends Biotechnol.* **2011**, *29* (4), 183-190.
- 13. Smith, C. M.; Stone, A. L.; Parkhill, R. L.; Stewart, R. L.; Simpkins, M. W.; Kachurin, A. M.; Warren, W. L.; Williams, S. K., Three-dimensional bioassembly tool for generating viable tissue-engineered constructs. *Tissue Eng.* **2004**, *10* (9-10), 1566-1576.
- 14. Campos, D. F. D.; Blaeser, A.; Weber, M.; Jäkel, J.; Neuss, S.; Jahnen-Dechent, W.; Fischer, H., Three-dimensional printing of stem cell-laden hydrogels submerged in a hydrophobic high-density fluid. *Biofabrication* **2012**, *5* (1), 015003.
- 15. Marga, F.; Jakab, K.; Khatiwala, C.; Shepherd, B.; Dorfman, S.; Hubbard, B.; Colbert, S.; Forgacs, G., Toward engineering functional organ modules by additive manufacturing. *Biofabrication* **2012**, *4* (2), 022001.
- 16. Chung, J. H.; Naficy, S.; Yue, Z.; Kapsa, R.; Quigley, A.; Moulton, S. E.; Wallace, G. G., Bio-ink properties and printability for extrusion printing living cells. *Biomaterials Science* **2013**, *1* (7), 763-773.
- 17. Dababneh, A. B.; Ozbolat, I. T., Bioprinting technology: a current state-of-the-art review. *Journal of Manufacturing Science and Engineering* **2014**, *136* (6), 061016.
- 18. Gungor-Ozkerim, P. S.; Inci, I.; Zhang, Y. S.; Khademhosseini, A.; Dokmeci, M. R., Bioinks for 3D bioprinting: an overview. *Biomaterials Science* **2018**, *6* (5), 915-946.
- 19. Gopinathan, J.; Noh, I., Recent trends in bioinks for 3D printing. *Biomater Res* **2018**, *22*, 11-11.
- 20. Panwar, A.; Tan, L. P., Current Status of Bioinks for Micro-Extrusion-Based 3D Bioprinting. *Molecules* **2016**, *21* (6), 685.
- 21. Adepu, S.; Dhiman, N.; Laha, A.; Sharma, C. S.; Ramakrishna, S.; Khandelwal, M., Three-dimensional bioprinting for bone tissue regeneration. *Current Opinion in Biomedical Engineering* **2017**, *2*, 22-28.
- 22. Pescosolido, L.; Vermonden, T.; Malda, J.; Censi, R.; Dhert, W. J. A.; Alhaique, F.; Hennink, W. E.; Matricardi, P., In situ forming IPN hydrogels of calcium alginate and dextran-HEMA for biomedical applications. *Acta Biomater.* **2011,** *7* (4), 1627-1633.
- 23. Park, J.; Lee, S. J.; Chung, S.; Lee, J. H.; Kim, W. D.; Lee, J. Y.; Park, S. A., Cellladen 3D bioprinting hydrogel matrix depending on different compositions for soft tissue

- engineering: Characterization and evaluation. *Materials Science and Engineering: C* **2017,** *71*, 678-684.
- 24. Hernández-González, A. C.; Téllez-Jurado, L.; Rodríguez-Lorenzo, L. M., Alginate hydrogels for bone tissue engineering, from injectables to bioprinting: A review. *Carbohydr. Polym.* **2020**, *229*, 115514.
- 25. Irmak, G. l.; Demirtaş, T. r. T.; Gümüşderelioğlu, M. e., Highly Methacrylated Gelatin Bioink for Bone Tissue Engineering. *ACS Biomaterials Science & Engineering* **2018**, *5* (2), 831-845.
- 26. Roehm, K. D.; Madihally, S. V., Bioprinted chitosan-gelatin thermosensitive hydrogels using an inexpensive 3D printer. *Biofabrication* **2017**, *10* (1), 015002.
- 27. Byambaa, B.; Annabi, N.; Yue, K.; Trujillo-de Santiago, G.; Alvarez, M. M.; Jia, W.; Kazemzadeh-Narbat, M.; Shin, S. R.; Tamayol, A.; Khademhosseini, A., Bioprinted Osteogenic and Vasculogenic Patterns for Engineering 3D Bone Tissue. *Advanced Healthcare Materials* **2017**, *6* (16), 1700015.
- 28. Das, S.; Pati, F.; Choi, Y.-J.; Rijal, G.; Shim, J.-H.; Kim, S. W.; Ray, A. R.; Cho, D.-W.; Ghosh, S., Bioprintable, cell-laden silk fibroin–gelatin hydrogel supporting multilineage differentiation of stem cells for fabrication of three-dimensional tissue constructs. *Acta Biomater*. **2015**, *11*, 233-246.
- 29. Kuss, M. A.; Harms, R.; Wu, S.; Wang, Y.; Untrauer, J. B.; Carlson, M. A.; Duan, B., Short-term hypoxic preconditioning promotes prevascularization in 3D bioprinted bone constructs with stromal vascular fraction derived cells. *RSC Advances* **2017**, *7* (47), 29312-29320.
- 30. O'Connell, C. D.; Di Bella, C.; Thompson, F.; Augustine, C.; Beirne, S.; Cornock, R.; Richards, C. J.; Chung, J.; Gambhir, S.; Yue, Z.; Bourke, J.; Zhang, B.; Taylor, A.; Quigley, A.; Kapsa, R.; Choong, P.; Wallace, G. G., Development of the Biopen: a handheld device for surgical printing of adipose stem cells at a chondral wound site. *Biofabrication* **2016**, *8* (1), 015019.
- 31. Kim, W. J.; Yun, H.-S.; Kim, G. H., An innovative cell-laden α -TCP/collagen scaffold fabricated using a two-step printing process for potential application in regenerating hard tissues. *Scientific reports* **2017**, *7* (1), 1-12.
- 32. Tozzi, G.; De Mori, A.; Oliveira, A.; Roldo, M., Composite hydrogels for bone regeneration. *Materials* **2016**, *9* (4), 267.
- 33. Bai, X.; Gao, M.; Syed, S.; Zhuang, J.; Xu, X.; Zhang, X.-Q., Bioactive hydrogels for bone regeneration. *Bioactive Materials* **2018**, *3* (4), 401-417.
- 34. Maturavongsadit, P.; Paravyan, G.; Shrivastava, R.; Benhabbour, S. R., Thermo-/pH-Responsive Chitosan-Cellulose Nanocrystal Based Hydrogel with Tunable Mechanical Properties for Tissue Regeneration Applications. *Materialia* **2020**, 100681.
- 35. Alinejad, Y.; Adoungotchodo, A.; Hui, E.; Zehtabi, F.; Lerouge, S., An injectable chitosan/chondroitin sulfate hydrogel with tunable mechanical properties for cell therapy/tissue engineering. *Int. J. Biol. Macromol.* **2018**, *113*, 132-141.
- 36. Cao, L.; Werkmeister, J. A.; Wang, J.; Glattauer, V.; McLean, K. M.; Liu, C., Bone regeneration using photocrosslinked hydrogel incorporating rhBMP-2 loaded 2-N, 6-O-sulfated chitosan nanoparticles. *Biomaterials* **2014**, *35* (9), 2730-2742.
- 37. Cui, Z.-K.; Kim, S.; Baljon, J. J.; Wu, B. M.; Aghaloo, T.; Lee, M., Microporous methacrylated glycol chitosan-montmorillonite nanocomposite hydrogel for bone tissue engineering. *Nature Communications* **2019**, *10* (1), 3523.

- 38. Kean, T.; Thanou, M., Biodegradation, biodistribution and toxicity of chitosan. *Adv. Drug Del. Rev.* **2010**, *62* (1), 3-11.
- 39. Xu, Y.; Han, J.; Chai, Y.; Yuan, S.; Lin, H.; Zhang, X., Development of porous chitosan/tripolyphosphate scaffolds with tunable uncross-linking primary amine content for bone tissue engineering. *Materials Science and Engineering: C* **2018**, *85*, 182-190.
- 40. Muzzarelli, R. A.; El Mehtedi, M.; Bottegoni, C.; Aquili, A.; Gigante, A., Genipin-Crosslinked Chitosan Gels and Scaffolds for Tissue Engineering and Regeneration of Cartilage and Bone. *Mar Drugs* **2015**, *13* (12), 7314-38.
- 41. Wang, L.; Stegemann, J. P., Glyoxal crosslinking of cell-seeded chitosan/collagen hydrogels for bone regeneration. *Acta Biomater.* **2011**, *7* (6), 2410-2417.
- 42. Kruyt, M.; De Bruijn, J.; Rouwkema, J.; Van Bliterswijk, C.; Oner, C.; Verbout, A.; Dhert, W., Analysis of the Dynamics of Bone Formation, Effect of Cell Seeding Density, and Potential of Allogeneic Cells in Cell-Based Bone Tissue Engineering in Goats. *Tissue Engineering Part A* **2008**, *14* (6), 1081-1088.
- 43. Zhai, X.; Ruan, C.; Ma, Y.; Cheng, D.; Wu, M.; Liu, W.; Zhao, X.; Pan, H.; Lu, W. W., 3D-Bioprinted Osteoblast-Laden Nanocomposite Hydrogel Constructs with Induced Microenvironments Promote Cell Viability, Differentiation, and Osteogenesis both In Vitro and In Vivo. *Advanced Science* **2018**, *5* (3), 1700550.
- 44. Ong, S.-M.; Zhang, C.; Toh, Y.-C.; Kim, S. H.; Foo, H. L.; Tan, C. H.; van Noort, D.; Park, S.; Yu, H., A gel-free 3D microfluidic cell culture system. *Biomaterials* **2008**, *29* (22), 3237-3244.
- 45. Chenite, A.; Buschmann, M.; Wang, D.; Chaput, C.; Kandani, N., Rheological characterisation of thermogelling chitosan/glycerol-phosphate solutions. *Carbohydr. Polym.* **2001**, *46* (1), 39-47.
- 46. Kempe, S.; Metz, H.; Bastrop, M.; Hvilsom, A.; Contri, R. V.; Mäder, K., Characterization of thermosensitive chitosan-based hydrogels by rheology and electron paramagnetic resonance spectroscopy. *Eur. J. Pharm. Biopharm.* **2008**, *68* (1), 26-33.
- 47. Hoemann, C. D.; Chenite, A.; Sun, J.; Hurtig, M.; Serreqi, A.; Lu, Z.; Rossomacha, E.; Buschmann, M. D., Cytocompatible gel formation of chitosan-glycerol phosphate solutions supplemented with hydroxyl ethyl cellulose is due to the presence of glyoxal. *Journal of Biomedical Materials Research Part A* **2007**, 83A (2), 521-529.
- 48. Demirtaş, T. T.; Irmak, G.; Gümüşderelioğlu, M., A bioprintable form of chitosan hydrogel for bone tissue engineering. *Biofabrication* **2017**, *9* (3), 035003.
- 49. Ng, W. L.; Yeong, W. Y.; Naing, M. W., Polyelectrolyte gelatin-chitosan hydrogel optimized for 3D bioprinting in skin tissue engineering. *International Journal of Bioprinting* **2016**, *2* (1), 53-62.
- 50. Li, C.; Wang, K.; Zhou, X.; Li, T.; Xu, Y.; Qiang, L.; Peng, M.; Xu, Y.; Xie, L.; He, C., Controllable fabrication of hydroxybutyl chitosan/oxidized chondroitin sulfate hydrogels by 3D bioprinting technique for cartilage tissue engineering. *Biomedical Materials* **2019**, *14* (2), 025006.
- 51. Hölzl, K.; Lin, S.; Tytgat, L.; Van Vlierberghe, S.; Gu, L.; Ovsianikov, A., Bioink properties before, during and after 3D bioprinting. *Biofabrication* **2016**, *8* (3), 032002.
- 52. Ozbolat, I. T.; Moncal, K. K.; Gudapati, H., Evaluation of bioprinter technologies. *Additive Manufacturing* **2017**, *13*, 179-200.
- 53. Ozbolat, I. T.; Peng, W.; Ozbolat, V., Application areas of 3D bioprinting. *Drug Discovery Today* **2016**, *21* (8), 1257-1271.

- 54. Ching, Y. C.; Ershad Ali, M.; Abdullah, L. C.; Choo, K. W.; Kuan, Y. C.; Julaihi, S. J.; Chuah, C. H.; Liou, N.-S., Rheological properties of cellulose nanocrystal-embedded polymer composites: a review. *Cellulose* **2016**, *23* (2), 1011-1030.
- 55. Hong, T.; Iwashita, K.; Shiraki, K., Viscosity Control of Protein Solution by Small Solutes: A Review. *Curr. Protein Peptide Sci.* **2018**, *19* (8), 746-758.
- 56. Skardal, A.; Zhang, J.; Prestwich, G. D., Bioprinting vessel-like constructs using hyaluronan hydrogels crosslinked with tetrahedral polyethylene glycol tetracrylates. *Biomaterials* **2010**, *31* (24), 6173-6181.
- 57. Buckley, C. T.; Thorpe, S. D.; O'Brien, F. J.; Robinson, A. J.; Kelly, D. J., The effect of concentration, thermal history and cell seeding density on the initial mechanical properties of agarose hydrogels. *Journal of the Mechanical Behavior of Biomedical Materials* **2009**, *2* (5), 512-521.
- 58. Müller, M.; Becher, J.; Schnabelrauch, M.; Zenobi-Wong, M., Nanostructured Pluronic hydrogels as bioinks for 3D bioprinting. *Biofabrication* **2015**, *7* (3), 035006.
- 59. Wang, L. L.; Highley, C. B.; Yeh, Y. C.; Galarraga, J. H.; Uman, S.; Burdick, J. A., Three-dimensional extrusion bioprinting of single-and double-network hydrogels containing dynamic covalent crosslinks. *Journal of Biomedical Materials Research Part A* **2018**, *106* (4), 865-875.
- 60. Kiyotake, E. A.; Douglas, A. W.; Thomas, E. E.; Nimmo, S. L.; Detamore, M. S., Development and quantitative characterization of the precursor rheology of hyaluronic acid hydrogels for bioprinting. *Acta Biomater.* **2019**, *95*, 176-187.
- 61. Paxton, N.; Smolan, W.; Böck, T.; Melchels, F.; Groll, J.; Jungst, T., Proposal to assess printability of bioinks for extrusion-based bioprinting and evaluation of rheological properties governing bioprintability. *Biofabrication* **2017**, *9* (4), 044107.
- 62. Nair, K.; Gandhi, M.; Khalil, S.; Yan, K. C.; Marcolongo, M.; Barbee, K.; Sun, W., Characterization of cell viability during bioprinting processes. *Biotechnology Journal: Healthcare Nutrition Technology* **2009**, *4* (8), 1168-1177.
- 63. Blaeser, A.; Duarte Campos, D. F.; Puster, U.; Richtering, W.; Stevens, M. M.; Fischer, H., Controlling shear stress in 3D bioprinting is a key factor to balance printing resolution and stem cell integrity. *Advanced Healthcare Materials* **2016**, *5* (3), 326-333.
- 64. Yeh, H.-Y.; Liu, B.-H.; Sieber, M.; Hsu, S.-h., Substrate-dependent gene regulation of self-assembled human MSC spheroids on chitosan membranes. *BMC Genomics* **2014**, *15* (1), 10.
- 65. Hsu, S.-h.; Huang, G.-S.; Feng, F., Isolation of the multipotent MSC subpopulation from human gingival fibroblasts by culturing on chitosan membranes. *Biomaterials* **2012**, *33* (9), 2642-2655.
- 66. Asghari Sana, F.; Çapkın Yurtsever, M.; Kaynak Bayrak, G.; Tunçay, E. Ö.; Kiremitçi, A. S.; Gümüşderelioğlu, M., Spreading, proliferation and differentiation of human dental pulp stem cells on chitosan scaffolds immobilized with RGD or fibronectin. *Cytotechnology* **2017**, *69* (4), 617-630.
- 67. Murphy, W. L.; McDevitt, T. C.; Engler, A. J., Materials as stem cell regulators. *Nature materials* **2014**, *13*, 547.